Antisolvent Crystallization Approach to Construction of CuI Superstructures with Defined Geometries

Rajeevan Kozhummal,[†,‡] Yang Yang,[†,*] Firat Güder,[†] Umut M. Küçükbayrak,[†] and Margit Zacharias[†,‡]

[†]Nanotechnology, Institute of Microsystems Engineering (IMTEK), Albert Ludwigs University of Freiburg, Georges-Köhler-Allee 103, D-79110 Freiburg, Germany and
[‡]School of Soft Matter Research, Freiburg Institute for Advanced Studies (FRIAS), Albert Ludwigs University of Freiburg, Albertstraße 19, D-79104 Freiburg, Germany

ABSTRACT A facile high-yield production of cuprous iodide (CuI) superstructures is reported by antisolvent crystallization using acetonitrile/water as a solvent/antisolvent couple under ambient conditions. In the presence of trace water, the metastable water droplets act as templates to induce the precipitation of hollow spherical CuI superstructures consisting of orderly aligned building blocks after drop coating. With water in excess in the mixed solution, an instant precipitation of CuI random aggregates takes place due to rapid crystal growth *via* ion-by-ion attachment induced by a strong antisolvent effect. However, this uncontrolled process can be modified by adding polymer polyvinyl pyrrolidone (PVP) in water to restrict the size of initially formed CuI crystal nuclei through the effective coordination effect of PVP. As a result, CuI superstructures with a cuboid geometry are constructed by gradual self-assembly of the small CuI crystals *via* oriented attachment. The precipitated CuI superstructures have been used as competent adsorbents to remove organic dyes from the water due to their mesocrystal feature. Besides, the CuI superstructures have been applied either as a self-sacrificial template or only as a structuring template for the flexible design of other porous materials such as CuO and TiO_2. This system provides an ideal platform to simultaneously investigate the superstructure formation enforced by antisolvent crystallization with and without organic additives.

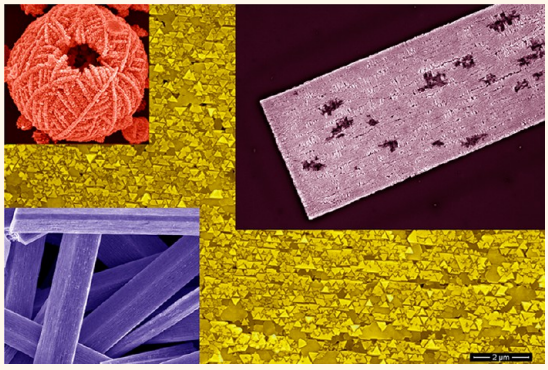

KEYWORDS: cuprous iodide · superstructures · antisolvent crystallization · organic additives · adsorbent

Superstructures constructed by small nanocrystal units *via* bottom-up approaches are a new type of nanostructured matter with potentially inspiring applications, which have been intensively investigated in recent years.[1−10] The building blocks which are uniform in size and shape usually lead to the formation of nanocrystal superlattices with high crystallographic symmetry, analogous to the alignment of atoms or molecules in the classical crystallization process.[8−10] However, when the starting units are nonspherical and polydispersed, superstructures with plentiful intrinsic defects, for instance in the form of mesocrystal, are often constructed either as an intermediate or as the final product.[1,3,5,7] It has been generally acknowledged that organic additives can significantly influence the nucleation, evolution, and organized aggregation of such superstructures by altering the surface energies, controlling the interspaces, and regulating the orientational order of the adjacent nanocrystal building units. There exist a large amount of examples in the processes of biomineralization in nature, where defined organic−inorganic hybrid superstructures with complex morphologies and hierarchical order are presented. Therefore, optimal design of artificial superstructures has largely been conducted by introducing organic additives with specific functional groups during the synthesis of nanocrystal building blocks by mimicking the biomineralization process.[1−5,11−13]

Nevertheless, it has also been reported that organic additives are not always necessary for the construction of nanocrystal superstructures especially when a high orientation consistency among the building blocks does not become a major concern. One recent example is the formation of strontium

* Address correspondence to yang.yang@imtek.de.

Received for review January 24, 2013 and accepted February 25, 2013.

Published online February 26, 2013
10.1021/nn4003902

sodium tantalite mesocrystals *via* an organic-additive-free molten salt process, where the molten salt restrains the further growth of the small building units and enhances their dipole field during the oriented aggregation process.[14] Another encouraging example is the construction of superstructures consisting of hopper-like single crystals of sodium chloride exploiting metastable water droplets as the template by antisolvent crystallization.[15] This strategy proceeded almost in a "nonreactive" route, avoiding any harsh chemical reactions as well as related byproducts. However, due to the nature of alkali metal ions which are inert to most organic ligands, it is not realistic to further modify this system by introducing functional organic additives as structure-directing agents for tuning the organization of the building blocks.

Low temperature (below 390 °C) γ-phase cuprous iodide (CuI) is an important p-type semiconducting binary metal halide with a large band gap of 3.1 eV. Synthesis of large single crystals,[16−18] high-quality thin films,[19−22] and low-dimensional nanostructures of CuI[23−29] has attracted much attention in recent years. However, so far the formation of CuI superstructures has not been reported. It is known that CuI is a water insoluble solid (pK_{sp} = 11.96) at room temperature. In contrast, acetonitrile (CH_3CN) is a good solvent for the dissolution of CuI because acetonitrile can strongly solvate CuI by reducing the Cu−I bond, and lead to the formation of CuI−acetonitrile adducts. The coordination originates from a significant π^* antibonding from cuprous to nitrogen atoms of acetonitrile. Herein, starting from commercial CuI powders, we report a facile and mild antisolvent crystallization approach for the construction of CuI superstructures by employing acetonitrile/water as a solvent/antisolvent couple. It will be demonstrated that the metastable water droplets can be used as templates to form spherical CuI superstructures with orderly aligned building blocks under optimal conditions. Furthermore, due to the coordination effect favored by the d^{10} electronic configuration of Cu(I), the antisolvent crystallization of CuI can be sufficiently modified by introducing specific organic additives for achieving CuI superstructures with other geometries. This system provides an ideal platform to simultaneously investigate the superstructure formation enforced by antisolvent crystallization with and without organic additives, which will enhance our understanding on how to design functional superstructures with desired crystal morphologies.

RESULTS AND DISCUSSION

The as-received commercial CuI powder is composed of random aggregates in a size range of several tens of micrometers. When the powder was dispersed in moisture-free acetonitrile in air (6.0 g/L, unsaturated), a transparent pale-yellow solution was formed. Drop coating this solution on a silicon substrate resulted in

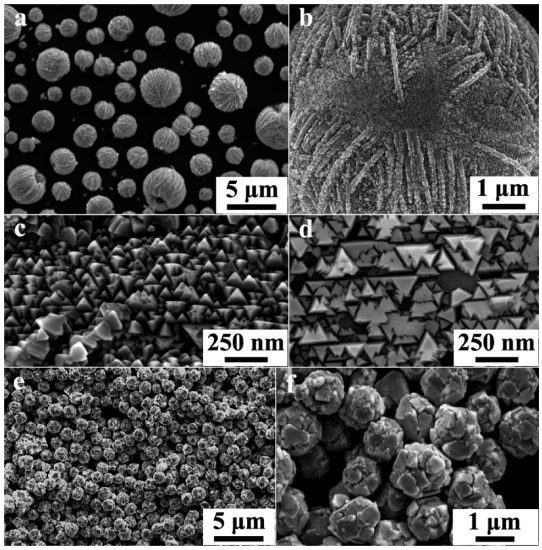

Figure 1. SEM images of (a) CuI microspheres obtained by drop coating of trace-water-added CuI acetonitrile solution on silicon substrates at room temperature, (b) the surface of a single CuI sphere, and (c,d) zoomed surface areas. SEM images of CuI precipitates obtained by injecting excess water into the CuI acetonitrile solution: (e) overview; (f) close view.

the formation of microsized single-crystalline CuI grains with a cubic shape together with some irregular aggregates, consistent with a previous report.[19] When 0.1 mL of water was added into 10 mL of the above CuI solution, polydispersed spherical particles with a hollow interior occurred through the same drop coating procedure, as shown in Figure 1a. These hollow spheres with a "sinkhole" are very similar to particles obtained by a spray drying process,[30] indicating a significant effect of trace water on the morphology of the CuI product *via* solvent evaporation. Figure 1b shows a close view of an individual CuI hollow sphere, in which a highly wrinkled surface is observed. Zooming on the unfolded areas of the surface, it is interesting to find that these flat areas are indeed composed of many small tetrahedral or truncated tetrahedral CuI building blocks with an average size of 80 nm (Figure 1c,d). The tips of an array of CuI blocks face either outward (Figure 1c) or inward (Figure 1d) to the sphere surface. The arrangement in each array is very compact with narrow gaps. The corresponding sides of most building units are parallel, indicating the formation of CuI superstructures with a relatively long-range order.

It can be assumed that initially the solvation of CuI in the liquid film was hardly influenced by trace water because the solvent acetonitrile was sufficient. Relative to water, acetonitrile is easy to vaporize due to its lower boiling point and smaller specific heat capacity. Therefore, the solution film on the substrate was gradually dispersed into water-rich metastable droplets with the preferential evaporation of acetonitrile in the mixture. Once supersaturation was reached, homogeneous nucleation of CuI happened at multiple sites all over the

droplet surface. Each CuI nucleus could continue to grow by sustainable supply of the CuI nutrient from the metastable water/acetonitrile droplets. After the remaining water in the center was finally vaporized, the CuI hollow spheres were formed.

Low temperature γ-phase CuI has the zinc blende-type cubic structure. Formation of tetrahedral nuclei with the zinc blende crystal structure is favored because the tetrahedral configuration exposes only close-packed {111} facets with the lowest surface energy.[21,26,27] Therefore, it is reasonable to form tetrahedral-shaped CuI crystals in the shell. The controlled alignment of tetrahedral-shaped CuI nanocrystals in the sphere shells was supposed to be favored by the air/droplet interface, which could provide an active platform to regulate the self-assembling behavior of the building blocks. However, the difference in boiling points and specific heat capacities of acetonitrile and water could induce different latent heat of evaporation and drying rates.[30] Therefore, the CuI shell was forced to fold during its growth for releasing the unbalanced stress, which led to the highly wrinkled surface.

The morphologies of the final products were not altered when the concentration of CuI acetonitrile solution was decreased to 3.0 g/L or increased to 12.0 g/L. Alternatively, when only 0.02 mL of water was added in 10 mL of 6.0 g/L CuI acetonitrile solution, the similar wrinkled hollow spheres were exclusively obtained as well. Hence, the trace water could affect the deposition of the CuI film in a large component range. However, when 3 mL of water was rapidly injected into 1 mL of 6.0 g/L CuI acetonitrile solution under vigorous stirring, a large amount of white precipitates instantly formed due to the strong antisolvent effect of the excess water. Figure 1e shows a typical SEM image of the product, in which uniform spherical solids with an average size of 1 μm are presented. Each sphere is indeed an aggregate consisting of many irregular CuI crystals with different sizes, clearly illustrated in Figure 1f. Inverse injection of CuI acetonitrile solution into the same amount of water led to a similar product.

The strong interaction between the water molecule and the acetonitrile molecule *via* hydrogen bonding would severely weaken the solvation of CuI when the CuI acetonitrile solution was rapidly injected into sufficient pure water or inversely. The attainment of supersaturation of CuI in the mixed solvents led to homogeneous nucleation of CuI clusters in the solution because the supersaturated solution is not energetically stable. The tetrahedral nuclei quickly grew into large particles by an alternative arrangement of I^- ions and Cu^+ ion at the interface based on classical crystallization. Tens of large particles further randomly aggregated into one spherical structure for reducing the surface area and finally precipitated.

Nitrogen-containing polymers such as PVP and PANI have been known as efficient matrices for the dispersion of CuI nanocrystallites.[24,29] The strong coordination effect between nitrogen atoms and Cu(I) ions can stabilize the crystallite surface, which is analogous to the solvation of CuI induced by acetonitrile. For investigating the effect of organic additives on the antisolvent crystallization of CuI, we selected PVP aqueous solution instead of pure water to mix with the CuI acetonitrile solution. Shortly after 1 mL of CuI acetonitrile solution (6.0 g/L) was injected into 3 mL of PVP aqueous solution (68.2 g/L) under vigorous magnetic stirring at room temperature, the mixed solution remained transparent. Colloidal precipitates gradually appeared about 30 min later under continuous stirring. XRD measurements confirmed that the deposited solids were CuI with zinc blende-type cubic structure (data not shown here). No other crystallized impurities were detected.

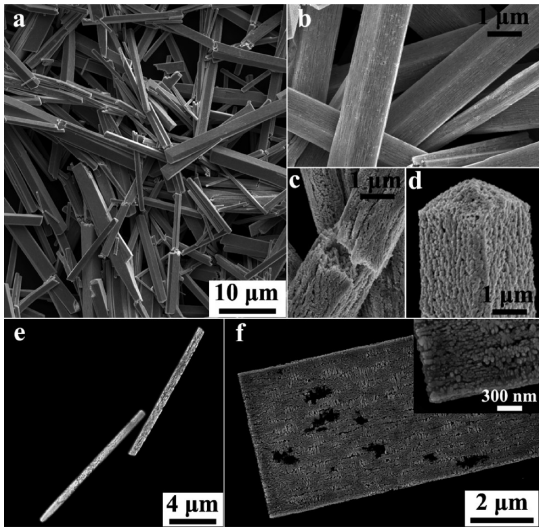

Figure 2. SEM images of rodlike CuI superstructures obtained by injecting 1 mL of CuI acetonitrile (6.0 g/L) into 3 mL of PVP aqueous solution (68.2 g/L) through a syringe pinhole under vigorous magnetic stirring at room temperature: (a) overview; (b–d) close view on typical individual rods. (e) SEM image of rodlike CuI superstructures obtained by injecting 1 mL of CuI acetonitrile (6.0 g/L) into 3 mL of PVP aqueous solution (136.4 g/L). (f) SEM images of sheetlike CuI superstructures obtained by injecting 1 mL of CuI acetonitrile (12.0 g/L) into 3 mL of PVP aqueous solution (68.2 g/L). Inset is a magnified image of one corner of the structure.

Figure 2a shows an SEM image of the collected deposits. Different from the precipitates by antisolvent crystallization in the absence of PVP, the current product exhibits the profile of a rodlike structure with various lengths and diameters. On the basis of the observation of Figure 2b, it can be seen that most of the rods are well-defined with a cuboid shape. However, the surface of these faceted rods is not smooth and is full of hidden lines. Figure 2c presents another rodlike structure with a fracture section caused by the mechanical force. It is clear that both the exterior and the interior of the rod are composed of numerous

nanoparticles. The external morphologies of the rod tips are either flat or truncated (Figure 2d), implemented by the orientational alignment of small building units. The formation of the rodlike superstructures was not influenced by the injection sequence, injection speed, and solution temperature (examined up to 60 °C). However, the concentrations of both the PVP and CuI had a major effect on the final morphologies. When the concentration of the PVP aqueous solution was doubled, longer stirring time was required to make the precipitation happen, which accordingly led to a less amount of CuI rods with smaller diameters, as shown in Figure 2e. When the concentration of CuI in acetonitrile was increased, the precipitation appeared much more quickly. The dominant morphology became a very regular planar rectangle (SEM image in Figure 2f and its inset). The thickness of the sheetlike structure is only 100 nm, while its width and length are up to several and tens of micrometers, respectively. Although the right angles and parallel sides are well-defined, the fabric of this sheet is also small nanoparticle building blocks, similar to the above rodlike structures. Therefore, all the precipitates with defined geometries obtained in the presence of PVP are not single crystals, but superstructures arranged by small nanoparticles.

A typical TEM image of the rodlike superstructure is shown in Figure 3a. The surface of the rod is not crystallographically flat. The porous interiors could be revealed by the low contrast regions. The selected area electron diffraction (SAED) pattern for the entire rod in Figure 3b dominantly shows cubic symmetrical diffraction spots corresponding to the zinc-blende phase of CuI. Although a detectable orientational distortion or scattering of the diffraction spots are demonstrated, this result confirms a high orientational order of the CuI subunits in the rodlike superstructure. The SAED pattern additionally shows that the elongation of the rod is along one ⟨220⟩ direction. This is also a conclusion for all the rodlike structures during our TEM observation. In combination with the cuboid shape based on the SEM investigation (Figure 2b), the four side faces of the rod should be bound by two {001} and two {220} planes, as indicated by the diffraction pattern. When the electron beam was purposely focused on a small portion of the rod (Figure 3c), it was interesting to find the structure undergo an obvious degradation. The stem slightly shrank while many tiny nanoparticles were released from the beam-focusing area. The halo-like SAED pattern shown in Figure 3d evidence an amorphous phase of the residue after irradiation for 30 s by the focused electron beam. Foam-like pores are uniformly distributed throughout the remaining structure (Figure 3d), which are most probably composed of the PVP matrix. This result straightly indicates that a certain amount of the organic additive was included in the CuI superstructures during antisolvent crystallization.

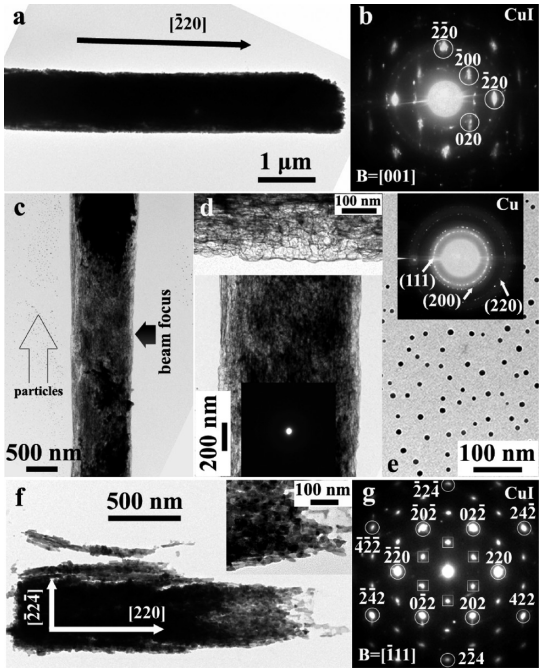

Figure 3. (a) TEM image and (b) corresponding SAED pattern of a rodlike CuI superstructure. (c) TEM image illustrating the irradiation of a focused electron beam on a selected portion after 30 s. (d) TEM images of the residual in the rod after beam irradiation. The inset is the SAED pattern of the bottom structure. (e) TEM image and corresponding SAED pattern (inset) of the released particles. (f) TEM image and (g) corresponding SAED pattern of a sheet-like CuI superstructure. The inset in panel f is a magnified view of its thinnest area. The spots marked by the cubic frames in the SAED pattern correspond to 1/3{422} reflections.

The released species are very tiny Cu nanoparticles due to the decomposition of CuI into Cu solid and iodine vapor induced by the focused electron beam in the TEM chamber, which is confirmed by the TEM image and its corresponding SAED pattern presented in Figure 3e.

Figure 3f shows a TEM image of a sheet-like superstructure with an imperfect appearance. Because the sheet-like structure is very thin, a better visualization of its internal configuration can be facilitated. It is found that some rod bundles partially merged into the sheet. A magnified region of the thinnest part of the sheet clearly reveals the brick-by-brick aggregation of small building units. The SAED pattern in Figure 3g was obtained by aligning the electron beam perpendicular to the planar surface. The diffraction spots with a 6-fold rotational symmetry originate from the zinc-blende phase of CuI, which confirms the highly oriented alignment of the CuI nanoparticles in this sheet-like structure. The long side of the observed sheet-like structures is all elongated along one ⟨220⟩ direction (exemplified in Figure 3g), agreeing with the rodlike superstructures. However, their flat top and bottom faces are always bound by two {111} planes. The existence of amplified 1/3{422} face-centered-cubic (FCC) reflections (marked by the cubic frames in Figure 3g) indicates the possibility of the presence of

multiple parallel twins on {111} planes parallel to the top and bottom surfaces of the lamellar structure.[31]

The {111} atomic planes of the tetrahedral CuI nuclei are polar, either negatively charged terminated by I^- ions or positively charged terminated by Cu^+ ions which are designated as the {222} planes. In the presence of polymer PVP, the {222} planes could be effectively stabilized due to the sufficient interaction between Cu^+ and the nitrogen atoms in PVP. Thus, the rapid growth of the critical crystal nuclei of CuI initiated by the antisolvent effect of water could be prevented. Moreover, the steric hindrance complied by the long-chain structure of PVP could retard the aggregation of these tiny CuI crystals. Therefore, after being mixed with the same volume of water, there were no immediate precipitates in the solution. With continuous vigorous stirring, these dispersed small blocks started to collide and fuse into each other. According to the surface energies associated with different crystallographic planes in the γ-phase CuI crystal lattice, the general sequence follows {111} < {100} < {110}. Therefore, these PVP-stabilized subunits could preferentially self-assemble along one ⟨220⟩ direction *via* oriented attachment possibly templated by PVP for minimizing the total free energy of the system.[32,33] The rodlike superstructures were gradually constructed and finally precipitated. Considering the random aggregates formed without PVP (Figure 1e,f), the formation of highly controlled alignment of CuI in the superstructures is greatly beneficial from the small sizes of the building units confined by PVP because the larger the grain is, the harder the oriented attachment is.[33] However, smaller crystal nuclei obtained by further increasing the concentration of PVP became more soluble, which accordingly restricted the evolution of the CuI superstructures by organized aggregation (Figure 2e). When the concentration of CuI was moderately increased, the coordination number of PVP at the rate-determining interfaces of the crystal nuclei was reduced, which led to the distribution of PVP more specific to certain planes. The 2-dimensional expansion based on the oriented attachment of the building blocks might become possible once an additional active plane was available. The sheet-like superstructures exhibited in our experiment hints that the oriented assembly also happened along one ⟨422⟩ direction in addition to the more preferred [220] direction in that case. A similar result was previously reported for the controlled dendritic growth of germanium with the FCC structure.[34] It was found that the principal surfaces of the long thin strips were bound to {111} crystallographic planes while the crystals grew rapidly in the [211] direction. The authors proposed that the presence of twin planes parallel to the flat surfaces was fundamental and necessary to this growth mode, which was expected to apply generally to materials with the zinc-blende structure.[34] Our structural observations for the sheet-like superstructure (Figure 3f,g) verifies that this mechanism is still valid for the nonclassic crystallization of superstructures by organized aggregation.

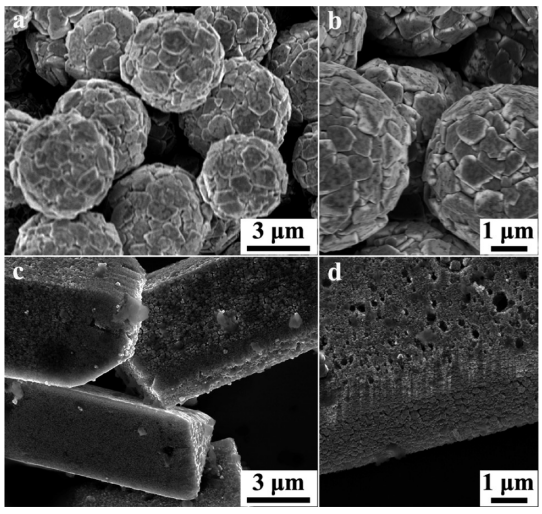

Figure 4. SEM images of CuI precipitates obtained by mixing 3 mL of Triton X-100 with the CuI acetonitrile solution: (a) overview; (b) close view. SEM images of CuI precipitates obtained by injecting 3 mL of PANI isopropyl alcohol solution (1.4 g/L) into the CuI acetonitrile solution: (c) overview; (d) close view.

The rodlike superstructures of CuI were stable at ambient conditions up to 6 months without any change of the geometries. The same stability was found after the CuI superstructures had been stored in water up to 3 months. However, when these structures were aged in the mother solution, a significant morphological transformation occurred within 72 h (data not shown). The surface of all the rods became very rough, decorated with many small particles or platelets. The faceted feature of the rods almost faded away. From a thermodynamics point of view, the cuboid rodlike superstructures are not stable because they are enclosed by the exposed planes with a high surface energy. Upon extended ripening in the mother solution, surface subunits with a relatively high mobility started to reconstruct based on the dissolution–recrystallization process, which finally eliminated the high-energy surfaces. This result implies that the CuI superstructures with well-defined geometries are kinetic, metastable intermediates rather than thermodynamically stable products.

For further investigation of the generality of this polymer-assisted antisolvent crystallization approach, other organic additives were also examined for the fabrication of CuI superstructures. When 3 mL of Triton X-100 was mixed with 1 mL of the CuI acetonitrile solution (6.0 g/L), spherical CuI aggregates consisting of randomly aligned crystals were quickly precipitated from the solution (Figure 4a,b). Injection of 3 mL of PANI isopropyl alcohol solution into the CuI acetonitrile solution caused rodlike CuI superstructures to

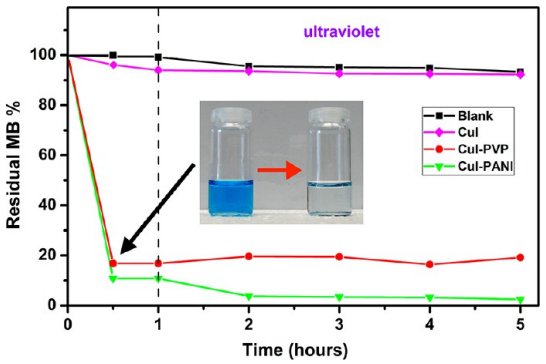

Figure 5. Adsorption rate of an aqueous solution of MB (4 mL, 6.4 g/L) for CuI-PVP and CuI-PANI rods, and for the as-received CuI powder. The mass of each sample was 10 mg. The photograph in the inset shows the color change of the MB solution before and 30 min after the addition of the CuI−PVP rods.

again form subsequent to a long-time stirring, as shown in Figure 4c. These rods are relatively shorter and thicker, but still very faceted with defined geometries (Figure 4d). The above results demonstrate the necessity of using organic additives with nitrogen-containing functional groups for modifying the anti-solvent crystallization of CuI from the acetonitrile solution.

Because the CuI building blocks have a polydispersed size distribution and surface defects, spaces were left among the particles even after their self-assembly into superstructures through lattice-matched surfaces.[35,36] Such an internal porous feature has been confirmed by our structural characterizations. For investigating the potential applications of the CuI porous superstructures in water treatment, the rodlike CuI superstructures induced by PVP and PANI (simplified as CuI-PVP and CuI-PANI, respectively) were used as adsorbents (10 mg) to remove the organic dye methylene blue (MB) (4 mL, 6.4 g/L) at room temperature. For comparison, the adsorption ability of the equal mass of the as-received CuI powder was also examined under the same adsorbing conditions. The adsorption experiments were first performed at ambient conditions and then continued under UV irradiation to distinguish the contribution of CuI as a possible photocatalyst. Figure 5 outlines the adsorption curves of all the tested samples. It can be found that the adsorption percentage of the CuI-PVP reached to 83% after 30 min (also refer to the photograph in the inset), accompanied by the attainment of the adsorption/desorption equilibrium. In contrast, the removal efficiency of the CuI-PANI reached to 90% after 30 min, which was further increased to 97% up to 2 h. The presence of the as-received CuI powder hardly reduced the concentration of MB even after long-time UV irradiation, indicating the negligible effect of CuI for the photocatalytic degradation of MB.[37] A large surface area derived from the high porosity is thus believed to be responsible for the efficient removal of MB by the CuI superstructures.[38,39]

Allowing for the reactivity of CuI at high temperatures, the CuI superstructures could further be used as self-sacrificial templates for conversion to other copper-derived functional materials. For instance, when the sphere-like CuI superstructures shown in Figure 1a were annealed in air at 400 °C for 1 h, highly porous CuO structures were formed, as exhibited in Figure 6a,b. The analogous transformation happened for the rodlike CuI superstructures as well (Figure 6c,d). Both the resultant CuO mesocrystals inherited the geometries of the starting CuI structures throughout oxidation, but of higher porosities. On the one hand, the oxidation of CuI or CuI-PVP to CuO led to a significant mass loss, which provided more free spaces in the stacking structures. Furthermore, it was revealed that the oxidation of each CuI building unit followed the nanoscale Kirkendall effect, by which a net outward flow of Cu^+ through the initially formed CuO shell could lead to an opposite transport of vacancies into the crystal interior, which would gradually condense into large voids.[26] The shell of the finally formed hollow CuO units was supposed to crack and dissociate into smaller subunits during the annealing at 400 °C. As evidenced in Figure 6b, most CuO nanoparticle aggregates on the surface of the CuO microspheres display the morphology of a tetrahedral cage, hence, maintaining the geometry of the initial CuI building blocks shown in Figure 1c. For this reason, the CuO hierarchical structures consist of smaller blocks and became much more porous.

Additionally, the CuI superstructures were employed as templates for the deposition of TiO_2 by ALD. In typical experiments, a TiO_2 layer with a thickness of 15 nm was deposited. In virtue of the good solubility of CuI in acetonitrile, the CuI templates were easily etched by acetonitrile at room temperature. Figure 6e shows an SEM image of the obtained TiO_2 structure by using hollow sphere-like CuI superstructure as the template, followed by the removal of CuI. The rugged surface feature indicates a large surface area compatible with the template morphology. A close view in Figure 6f confirms that each surface building unit has been conformally transformed into a hollow block due to the self-limiting surface reaction of ALD and the subsequent removal of CuI.[40] A similar replication was achieved when the rodlike CuI superstructures were used as the template. As clearly reflected in Figure 6g,h, the rodlike TiO_2 structures are porous, presenting a hierarchical interior and a foam-like surface. An obvious advantage of this route lies in the easy, mild, and specific removal of the CuI templates only by the neutral organic solvent acetonitrile, which is expected to be a general templating strategy for the fabrication of many other porous

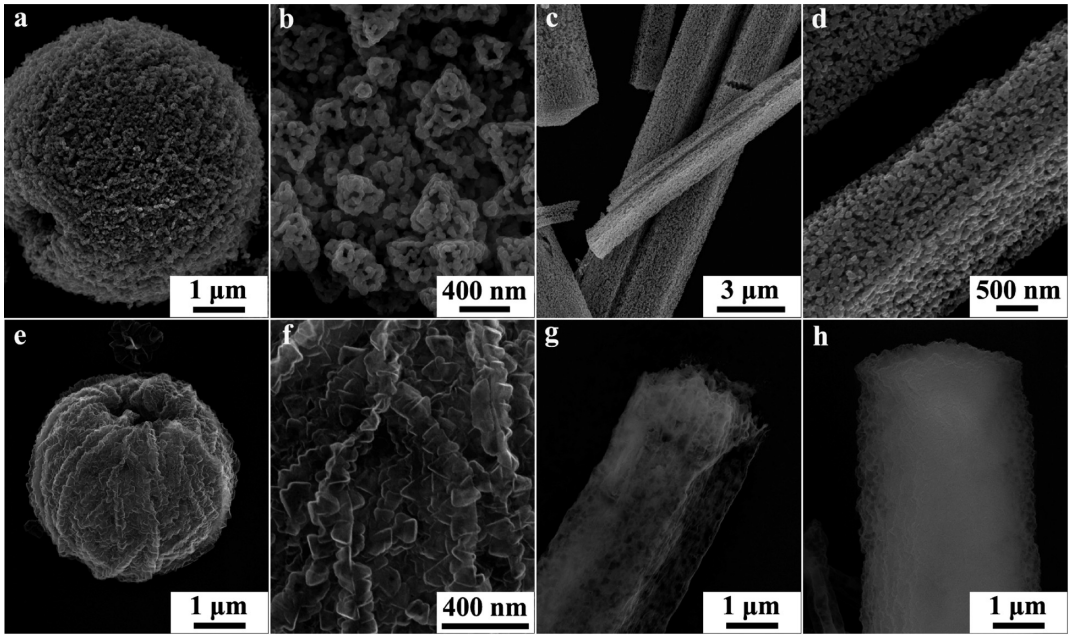

Figure 6. SEM images of the CuO structures obtained by annealing the sphere-like CuI superstructures, (a) overview, (b) close view, and the rodlike CuI superstructures, (c) overview, (d) close view, at 400 °C in air for 1 h. SEM images of the ALD-coated TiO_2 structures subjected to the etching of the sphere-like: (e) overview; (f) close view, and the rodlike CuI superstructure templates (g,h), in acetonitrile at room temperature. A total number of 1000 ALD cycles was applied at 150 °C for achieving the deposition of a TiO_2 layer with a thickness of 15 nm.

materials, especially in combination with the ALD technique.[40]

CONCLUSIONS

We have investigated the formation of CuI superstructures by antisolvent crystallization with and without organic additives. It is found that the presence of trace water can induce the formation of hollow sphere-like CuI superstructures by drop coating the CuI solution on a substrate. The gradually condensed metastable water droplets not only work as an antisolvent to help the precipitation of CuI nuclei with the evaporation of acetonitrile, but regulate their growth and arrangement at the droplet surface. For this reason, the finally formed sphere shells are composed of nanoscale tetrahedral CuI building blocks in an ordered alignment. When excess water is mixed with the CuI acetonitrile solution, spherical aggregates are instantly precipitated in the mixed solution due to the rapid growth of larger CuI crystals and subsequent random agglomeration. However, such simultaneous antisolvent precipitation does not take place in the presence of organic additives such as PVP. The strong stabilizing effect of PVP on the initially formed CuI crystal nuclei can restrict the crystal growth *via* ion-by-ion attachment. Afterward, small CuI crystals with a confined size only behave like building blocks and gradually self-assemble into CuI superstructures by oriented attachment. The finally precipitated CuI superstructures in the majority are cuboid mesocrystals with a well-defined geometry, which could be tuned by the PVP concentration and the molar ratio of CuI relative to PVP. This antisolvent crystallization approach is ideal to form CuI superstructures with tunable geometries in a single step with feasibility for large-scale production. Moreover, any harsh chemical reactions for the solidification of CuI crystals can be avoided by this route. Our proof-of-concept results have shown that the formed CuI mesocrystals can be used as competent adsorbents for the fast removal of organic dyes in water due to their high porosity. The CuI superstructures can also be applied either as a self-sacrificial template or only as a structuring template for the flexible design of other functional porous materials. Such an antisolvent crystallization approach is expected to be a general strategy for constructing superstructures of many other ionic compounds containing a transition metal.

EXPERIMENTAL SECTION

Materials. Cuprous iodide (CuI), polyvinyl pyrrolidone (PVP, average $M_W \approx 58\,000$), polyaniline (emeraldine base) (PANI, average $M_w \approx 50\,000$), Triton X-100, methylene blue (MB, $C_{16}H_{18}N_3SCl$), and acetonitrile (CH_3CN, 99.8%) were all analytical-grade reagents, procured from Sigma Aldrich and used without further purification. Deionized water was used to prepare all the aqueous solutions throughout the experiments.

Preparation of CuI Superstructures. Commercial CuI powder was dissolved in acetonitrile by ultrasonication for forming a

transparent solution with a concentration of 6.0 g/L (solution A). Then 0.1 mL of water was added into 10 mL of solution A under stirring. Several droplets of the above solution were dispersed onto a silicon piece and dried at ambient conditions. White residues appeared on the silicon substrate after the solvent was evaporated. In the next experiment, 3 mL of water was quickly injected into 1 mL of solution A through a syringe pinhole (B.Braun-Sterican, 0.6 mm outside diameter of the needle) under vigorous magnetic stirring. The rapidly formed white precipitates were filtered and washed with deionized water and ethanol, and dried at room temperature.

In a typical experiment in the presence of organic additives, 3 mL of PVP aqueous solution (68.2 g/L) was injected into 1 mL of solution A through the syringe pinhole under vigorous magnetic stirring. After 30 min, cloudy white precipitates were collected by the removal of supernatant, followed by washing with deionized water and ethanol, and drying at room temperature. This experiment was also conducted by changing the injection sequence, injection speed, solution temperature, and the concentration of PVP. In addition, the above procedure was performed by using 3 mL of Triton X-100 and 3 mL of PANI isopropyl alcohol solution (1.4 g/L), respectively, instead of the PVP solution.

To understand the growth process of the superstructures, the effects of the concentration of the CuI acetonitrile solution (solution A) on the morphology and size of the final products were continuously investigated during the above experiments as well.

Adsorption Experiments. Adsorption experiments were carried out at room temperature. The as-prepared CuI–PVP and CuI–PANI rodlike superstructures (10 mg) were respectively dispersed into 4 mL of 20 mM MB aqueous solution by vigorous shaking for 30 s and then left for a specified time. The equilibrium concentrations of MB solution were measured with a UV–vis spectrophotometer (Perkin-Elmer, Lambda 950) at a wavelength of 664 nm corresponding to the maximum absorbance of MB. For comparison, the adsorbing property of the same amount of as-received CuI powder was also examined *via* the same process.

Templating Experiments. For the conversion of CuI to CuO, CuI superstructures collected on silicon substrates were annealed in air in an open furnace at 400 °C for 1 h. For the application of CuI superstructures as templates for atomic layer deposition (ALD) of TiO_2, the deposition were conducted at 150 °C by reacting titanium isopropoxide with water vapor in a vertical flow type hot wall reactor (OpAL, Oxford Instruments). N_2 was used as the carrier gas with a flow rate of 100 sccm for this process. A total number of 1000 ALD cycles was applied to achieve the the deposition of a TiO_2 layer with a thickness of 15 nm. The TiO_2-coated samples were dipped into acetonitrile for 5 min at room temperature to remove the CuI and then dried in air.

Characterization. High-resolution SEM images were recorded using a Nova NanoSEM (FEI) equipped with an X-ray analyzer (EDX). Crystal structure was characterized by XRD θ–2θ scans using a Philips X'Pert MRD diffractometer with Cu Kα radiation. TEM images and corresponding ED patterns were obtained by using a JEOL 1010 microscope at an accelerating voltage of 100 kV.

Conflict of Interest: The authors declare no competing financial interest.

Acknowledgment. Financial support from German Research Foundation (DFG) under contract ZA 191/24-1 and Freiburg Institute for Advanced Studies (FRIAS) is gratefully acknowledged. We also thank Ms Anli Ding from IMTEK for her help for some preliminary experiments.

REFERENCES AND NOTES

1. Antonietti, M.; Göltner, C. Superstructures of Functional Colloids: Chemistry on the Nanometer Scale. *Angew. Chem., Int. Ed.* **1997**, *36*, 910–928.
2. Tang, Z.; Kotov, N. A.; Giersig, M. Spontaneous Organization of Single CdTe Nanoparticles into Luminescent Nanowires. *Science* **2002**, *297*, 237–240.
3. Cölfen, H.; Antonietti, M. Mesocrystals: Inorganic Superstructures Made by Highly Parallel Crystallization and Controlled Alignment. *Angew. Chem., Int. Ed.* **2005**, *44*, 5576–5591.
4. Tang, Z.; Zhang, Z.; Wang, Y.; Glotzer, S. C.; Kotov, N. A. Self-Assembly of CdTe Nanocrystals into Free-Floating Sheets. *Science* **2006**, *314*, 274–278.
5. Zhang, Q.; Liu, S. J.; Yu, S. H. Recent Advances in Oriented Attachment Growth and Synthesis of Functional Materials: Concept, Evidence, Mechanism, and Future. *J. Mater. Chem.* **2009**, *19*, 191–207.
6. Xia, Y.; Nguyen, T. D.; Yang, M.; Lee, B.; Santos, A.; Podsiadlo, P.; Tang, Z.; Glotzer, S. C.; Kotov, N. A. Self-Assembly of Self-Limiting Monodisperse Supraparticles from Polydisperse Nanoparticles. *Nat. Nanotechnol.* **2011**, *6*, 580–587.
7. Gao, Y.; Tang, Z. Design and Application of Inorganic Nanoparticle Superstructures: Current Status and Future Challenges. *Small* **2011**, *7*, 2133–2146.
8. Rogach, A. L.; Talapin, D. V.; Shevchenko, E. V.; Kornowski, A.; Haase, M.; Weller, H. Organization of Matter on Different Size Scales: Monodisperse Nanocrystals and Their Superstructures. *Adv. Func. Mater.* **2002**, *12*, 653–664.
9. Xia, Y.; Tang, Z. Monodisperse Inorganic Supraparticles: Formation Mechanism, Properties and Applications. *Chem. Commun.* **2012**, *48*, 6320–6336.
10. Gong, J.; Li, G.; Tang, Z. Self-Assembly of Noble Metal Nanocrystals: Fabrication, Optical Property, and Application. *Nano Today* **2012**, *7*, 564–585.
11. Mann, S.; Archibald, D. D.; Didymus, J. M.; Douglas, T.; Heywood, B. R.; Meldrum, F. C.; Reeves, N. J. Crystallization at Inorganic–Organic Interfaces: Biominerals and Biomimetic Synthesis. *Science* **1993**, *261*, 1286–1292.
12. Banfield, J. F.; Welch, S. A.; Zhang, H.; Ebert, T. T.; Penn, R. L. Aggregation-Based Crystal Growth and Microstructure Development in Natural Iron Oxyhydroxide Biomineralization Products. *Science* **2000**, *289*, 751–754.
13. Yu, S. H.; Cölfen, H.; Tauer, K.; Antonietti, M. Tectonic Arrangement of $BaCO_3$ Nanocrystals into Helices Induced by a Racemic Block Copolymer. *Nat. Mater.* **2005**, *4*, 51–55.
14. Sun, J.; Chen, G.; Pei, J.; Jin, R.; Wang, Q.; Guang, X. A Simple Approach to Strontium Sodium Tantalite Mesocrystals with Ultra-high Photocatalytic Properties for Water Splitting. *J. Mater. Chem.* **2012**, *22*, 5609–5614.
15. Zhang, J.; Zhang, S.; Wang, Z.; Zhang, Z.; Wang, S.; Wang, S. Hopper-like Single Crystals of Sodium Chloride Grown at the Interface of Metastable Water Droplets. *Angew. Chem., Int. Ed.* **2011**, *50*, 6044–6047.
16. Gao, P.; Gu, M.; Liu, X. L. Understanding the Growth Mechanism of CuI Crystals during Gel Growth Experiments. *Cryst. Res. Technol.* **2008**, *43*, 496–501.
17. Pan, J.; Yang, S.; Li, Y.; Han, L.; Li, X.; Cui, Y. CuI Crystal Growth in Acetonitrile Solvent by the Cycle-Evaporation Method. *Cryst. Growth Des.* **2009**, *9*, 3825–3827.
18. Chen, D.; Wang, Y.; Lin, Z.; Huang, J.; Chen, X.; Pan, D.; Huang, Feng. Growth Strategy and Physical Properties of the High Mobility P-Type CuI Crystal. *Cryst. Growth Des.* **2010**, *10*, 2057–2060.
19. Sirimanne, P. M.; Rusop, M.; Shirata, T.; Soga, T.; Jimbo, T. Characterization of CuI Thin Films Prepared by Different Techniques. *Mater. Chem. Phys.* **2003**, *80*, 461–465.
20. Yang, Y.; Gao, Q. Growth and Photoluminescence Characterization of Highly Oriented CuI/β-Cyclodextrin Hybrid Composite Film. *Langmuir* **2005**, *21*, 6866–6871.
21. Hu, X.; Yu, J. C.; Gong, J.; Li, Q. A Facile Surface-Etching Route to Thin Films of Metal Iodides. *Cryst. Growth Des.* **2007**, *7*, 262–267.
22. Zhou, Y.; Taima, T.; Miyadera, T.; Yamanari, T.; Kitamura, M.; Nakatsu, K.; Yoshida, Y. Glancing Angle Deposition of Copper Iodide Nanocrystals for Efficient Organic Photovoltaics. *Nano Lett.* **2012**, *12*, 4146–4152.
23. Fujimori, Y.; Gotoh, Y.; Tamaki, N.; Ohkoshi, Y.; Nagura, M. Introduction of Copper Iodide Fine Particles into a Poly(acrylic acid) Matrix *via* a Complex of Polymer–Polyiodide Ions. *J. Mater. Chem.* **2005**, *15*, 4816–4822.
24. Yang, Y.; Liu, S.; Kimura, K. A Facile Chemical Solution Route to Convert Bulk Cuprous Iodide into Nanoparticles. *Chem. Lett.* **2005**, *34*, 902–903.

25. Li, X.; Wan, M. Morphology and Hydrophobicity of Micro/Nanoscaled Cuprous Iodide Crystal. *Cryst. Growth Des.* **2006**, *6*, 2661–2666.
26. Ng, C. H. B.; Fan, W. Y. Facile Synthesis of Single-Crystalline γ-CuI Nanotetrahedrons and Their Induced Transformation to Tetrahedral CuO Nanocages. *J. Phys. Chem. C* **2007**, *111*, 9166–9171.
27. Zhang, B.; Xie, A.; Shen, Y.; Yang, L.; Huang, Y.; Lu, J. Morphogenesis of CuI Nanocrystals by a TSA-Assisted Photochemical Route: Synthesis, Optical Properties, and Growth Mechanism. *Eur. J. Inorg. Chem.* **2009**, *2009*, 1376–1384.
28. Meng, L. R.; Mo, R.; Zhou, H.; Wang, G.; Chen, W.; Wang, D.; Peng, Q. Synthesis of Luminescent Cubic Phase One-Dimensional CuI Nanostructures in Solution. *Cryst. Growth Des.* **2010**, *10*, 3387–3390.
29. Wang, X.; Shen, Y.; Xie, A.; Qiu, L.; Li, S.; Wang, Y. Novel Structure CuI/PANI Nanocomposites with Bifunctions: Superhydrophobicity, and Photocatalytic Activity. *J. Mater. Chem.* **2011**, *21*, 9641–9646.
30. Vehring, R. Pharmaceutical Particle Engineering *via* Spray Drying. *Pharm. Res.* **2008**, *25*, 999–1022.
31. Kirkland, A. I.; Jefferson, D. A.; Duff, D. G.; Edwards, P. P.; Gameson, I.; Johnson, B. F. G.; Smith, D. J. Structural Studies of Trigonal Lamellar Particles of Gold and Silver. *Proc. R. Soc. London A* **1993**, *440*, 589–609.
32. Penn, R. L.; Banfield, J. F. Imperfect Oriented Attachment: Dislocation Generation in Defect-free Nanocrystals. *Science* **1998**, *281*, 969–971.
33. Li, D.; Nielsen, M. H.; Lee, J. R. I.; Frandsen, C.; Banfield, J. F.; De Yoreo, J. J. Direction-Specific Interactions Control Crystal Growth by Oriented Attachment. *Science* **2012**, *336*, 1014–1018.
34. Bennett, A. I.; Longini, R. L. Dendritic Growth of Germanium Crystals. *Phys. Rev.* **1959**, *116*, 53–61.
35. Tan, H. R.; Tan, J. P. Y.; Boothroyd, C.; Hansen, T. W.; Foo, Y. L.; Lin, M. Experimental Evidence for Self-Assembly of CeO_2 Particles in Solution: Formation of Single-Crystalline Porous CeO_2 Nanocrystals. *J. Phys. Chem. C* **2012**, *116*, 242–247.
36. Zhan, H.; Yang, X.; Wang, C.; Chen, J.; Wen, Y.; Liang, C.; Greer, H. F.; Wu, M.; Zhou, W. Multiple Nucleation and Crystal Growth of Barium Titanate. *Cryst. Growth Des.* **2012**, *12*, 1247–1253.
37. Lv, B.; Cheng, C.; Yuan, H.; Xiao, D. *In Situ* Coordination of Pyridine, Quinoline, and Quinoxaline with Copper(I) Iodide at the Solid−Liquid Interface: Formation, Characterization, and Function of the Microcrystal Films. *J. Mater. Res.* **2008**, *23*, 1722–1731.
38. Liu, J.; Wan, Y.; Meng, F.; Huang, X.; Liu, J. Novel Hierarchically-Packed Tin Dioxide Sheets for Fast Adsorption of Organic Pollutant in Aqueous Solution. *J. Mater. Chem.* **2012**, *22*, 2885–2893.
39. Zhai, T.; Xie, S.; Lu, X.; Xiang, L.; Yu, M.; Li, W.; Liang, C.; Mo, C.; Zeng, F.; Luan, T.; Tong, Y. Porous $Pr(OH)_3$ Nanostructures as High-Efficiency Adsorbents for Dye Removal. *Langmuir* **2012**, *28*, 11078–11085.
40. Knez, M.; Nielsch, K.; Niinistö, L. Synthesis and Surface Engineering of Complex Nanostructures by Atomic Layer Deposition. *Adv. Mater.* **2007**, *19*, 3425–3438.